Constraint Evaluation and Effects on J-R resistance Curves for Pipes under Combined Load Conditions

Sebastian Cravero[1,a], Richard E. Bravo[1,b] and Hugo A. Ernst[1,c]

[1]TENARIS GROUP R&D Argentina - Dr. Simini 250, CP:2804, Campana – Argentina

[a]scravero@tenaris.com, [b]rbravo@tenaris.com, [c]hernst@tenaris.com

Keywords: crack tip constraint, biaxial load, resistance curve, crack growth

Abstract: Single edge cracked under tension (SENT) specimens appear as an alternative to conventional fracture specimens to characterize fracture toughness of circumferentially cracked pipes. The similarities of stress and strains fields between SENT specimens and cracked pipes are now well known. However, these similarities are not so well established for the case of circumferentially cracked pipes under combined loading conditions (i.e. internal pressure plus bending). This work presents a numerical analysis of crack-tip constraint of circumferentially surface cracked pipes and SENT specimens using full 3D nonlinear computations. The objective is to examine combined loading effects on the correlation of fracture behavior for the analyzed crack configurations. The constraint study using the J-Q methodology and the h parameter gives information about the fracture specimen that best represents the crack-tip conditions on circumferentially flawed pipes under combined loads. Additionally, simulations of ductile tearing in a surface cracked plate under biaxial loading using the computational cell methodology demonstrate the negligible effect of biaxial loadings on resistance curves.

Introduction

Structural defects in pressurized piping systems are very often surface cracks that form during fabrication or during in-service operation. The fracture conditions of these crack configurations contrast sharply to fracture conditions present in conventional deeply cracked specimens (i.e. CT or SENB). Single edge cracked under tension specimens (SENT) appear as an alternative to conventional fracture specimens to characterize fracture toughness of circumferentially cracked pipes. The similarities of stress and strains fields between SENT specimens and cracked pipes are now well determined. However, these similarities are not so well established for the case of circumferentially cracked pipes under combined load conditions (i.e. internal pressure plus tension, internal pressure plus bending, etc.). Heating and cooling cycles, ground movement and frost heave are examples of situations that produce yielding in the pipe metal when it is submitted to biaxial loading.

To further understand the effects of combined loading conditions on fracture behavior of flawed pipes, this work presents a numerical investigation of crack-tip constraint of circumferentially surface cracked pipes and SENT specimens using full 3D nonlinear computations. The primary objective is to examine combined loading effects on the correlation of fracture behavior for the analyzed crack configurations using the Q [1, 2] and h [3] parameters. The Q parameter measures the deviation of the stress field of the studied geometry from a reference stress solution (i.e. the boundary layer model [4]). On the other hand, the h parameter is defined as the ratio of the hydrostatic stress level ahead of the crack front over the effective Von Mises stress and it characterizes the growth of micro voids in a triaxial stress field. Furthermore, simulations of ductile tearing in a surface cracked plate under biaxial loading using the computational cell methodology allow the study of biaxial effects on tearing behavior. The constraint study and the crack growth

simulations set the basis for determination of the fracture specimen that best represents the crack-tip conditions on circumferentially flawed pipes.

FE Models for Stationary Cracks

FE models of clamped (no rotation at grips) SENT specimens and circumferentially cracked pipes were constructed. Figure 1-(a) shows the FE model constructed for the SENT geometry with a relative crack length of $a/W = 0.5$ the other considered crack size was $a/W = 0.15$. The width of the analyzed specimens is $W = 14.3$mm, the ratio of specimen thickness to specimen width is, $B/W = 2$, the relative specimen length is, $H/W = 10$. As in the SENT models, the 3D pipe models also have relative crack depths of $a/t = 0.15$ and 0.5 with crack depth to crack length ratio, $a/c = 0.3$ (a=2 mm, c=6.6 mm and a=7, c=23.33mm). The outside diameter and wall thickness of the studied pipes are 323.9 mm and 14.3 mm respectively. Figure 1-(b) shows one of the finite elements models constructed for the 3D analysis of the flawed pipes with $a/W = 0.5$.

In both geometries, reflective symmetry about the crack plane and the mid plane enables the use of one-quarter models as indicated in the Fig. 1 (a-b). The mesh of the finite elements models consists of 8−node, hexahedron isoparametric elements arranged in variable thickness layers. The thinner layers define the near free surface to resolve the strong variation of the stress and strain fields near the free face of the cracks. Within each layer, a sequence of focused rings of elements encloses the crack front. A small "key-hole" at the crack tip is used to simulate the initial blunting of the crack. The 3D SENT models have around 18,000 elements (20,000 nodes) and the 3D pipe models have around 22,000 elements (28,000 nodes).

In order to study the biaxial effects, the pipes are submitted to increasing curvature and different levels of internal pressure. The maximum curvature imposed to the pipes produces maximum longitudinal strains of around 2% at the outer fiber. These levels of deformations are more demanding than the actual strains accepted in a pipeline under service. However, the complete loading range (0-2%) is analyzed. The considered internal pressures produce circumferentially (hoop) stresses of 10, 20, 50 and 80% of the material yield stress.

The numerical computations for the fracture specimens and cracked pipes analyzed in this work are generated using the research code WARP3D [5]. The analyses utilize an elastic-plastic constitutive model with J_2 flow theory and conventional Mises plasticity using small strain theory. The numerical solutions employ a simple power-hardening model to characterize the uniaxial true stress-strain in the form

$$\frac{\varepsilon}{\varepsilon_0} = \frac{\sigma}{\sigma_0} \qquad \varepsilon \le \varepsilon_0; \quad \frac{\varepsilon}{\varepsilon_0} = \left(\frac{\sigma}{\sigma_0}\right)^n \qquad \varepsilon > \varepsilon_0 \tag{1}$$

where σ_0 and ε_0 are the reference (yield) stress and strain respectively and n is the strain hardening exponent. The finite element analyses consider material flow properties covering a typical X60 line pipe steel with $n = 10$ and $E/\sigma_0 = 500$. Here, $E = 210$ GPa and $\nu = 0.3$.

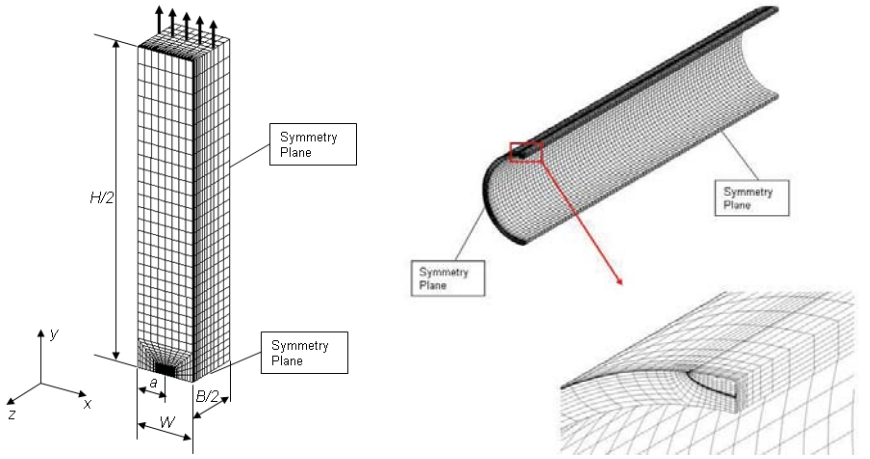

(a) (b)

Figure. 1: a) 3D finite element model of the SENT specimen with $a/W = 0.5$; b) 3D finite element model used in the analyses of the deeply cracked pipe ($a/t = 0.5$) with D = 323.9 mm and t = 14.3mm.

FE Models for Ductile Tearing using the Computational Cell Methodology

A semielliptical surface cracked plate under different levels of biaxial loading (Fig. 2) was constructed to simulate stable crack growth and to study the effect of biaxial loading on resistance curves. The simulation is based on the computational cell methodology proposed by Xia and Shih [6]. This methodology is used to predict ductile resistance curves of cracked specimens. The fracture is assumed to propagate in the plane containing the defect which is formed by computational cells with dimension D defining the thickness of the layer were the damage occurs. The cells have initial void volume fraction denoted by f_0, without subsequent void nucleation. Progressive void growth and macroscopic material softening in each cell are described with the Gurson-Tvergaard (GT) constitutive model [6, 7] given by

$$\Phi = \left(\frac{\sigma_e}{\bar{\sigma}}\right)^2 + 2q_1 f \cosh\left(\frac{3q_2\sigma_m}{2\bar{\sigma}}\right) - \left(1 + q_1^2 f^2\right) = 0 \qquad (2)$$

where σ_e denotes the effective Mises stress, σ_m is $\frac{1}{3}$ of the trace of the stress tensor (hydrostatic stress), $\bar{\sigma}$ is the current flow stress of the cell material and f defines the current void fraction. Factors q_1 and q_2, introduced by Tvergaard, improve the model predictions for interaction among multiple-voids. For the present study, typical values found in bibliography were considered for the calibration parameters of the computational cells [5], q_1=1.25, q_2=1.0, f_0=0.001 and D=0.2mm. Material outside the computational cell layer follows a conventional J_2 flow theory of plasticity and remains undamaged. The crack extension occurs when the current void fraction f reaches a critical value in any computational cell. In this case WARP3D eliminate the remaining nodal forces using a traction separation model. For additional information about the computational cell methodology, the reader can refer to the works of Xia and Shih [6] and Ruggieri and Dodds [7].

As for the deeply cracked pipe, the surface cracked plate have relative crack depth of a/t = 0.5 and a crack depth to crack length ratio, a/c = 0.3 (a=7 mm, c=23.33 mm). The width and thickness

of the studied plate are W = 50.0 mm and t = 14.3 mm respectively. Figure 2 shows the finite elements model constructed for simulating crack growth. Reflective symmetry about the crack plane and the mid plane enables the construction of one-quarter model as indicated in the figure. The crack front is made by consecutive layers constituted of 24 computational cells. The model has around 6,600 8-node brick elements.

In order to study the biaxial effects, the plate is subjected to increasing displacements in the direction normal to the crack plane and different levels of uniform stresses parallel to the crack plane (see Fig.2). The considered uniform stresses produce parallel stresses of 10, 20, 50 and 80% of the material yield stress.

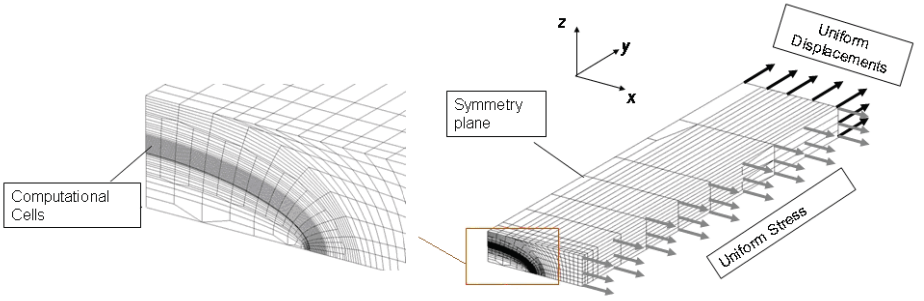

Figure 2: 3D finite element model used in ductile tearing analyses of surface cracked plate, a/t = 0.5 a/c = 0.3.

Applied *J* as a Function of Position along the Crack Front

With the previously presented numerical models, the applied *J*-integral is calculated at different positions over the crack front and loading conditions. Figure 3 presents applied *J*-integral as a function of positions over the crack front for the pipe with a/t = 0.5 (a =7 mm, c=23.33 mm) and 2% of deformation at the outer fiber without internal pressure. Because of the strong variation of *J* near free surfaces of the defect, it is uncertain what is the appropriate value of *J* to be employed for characterizing the crack loading condition. Since the fracture initiation is a local phenomenon, it is reasonable to use a local value of *J* instead an averaged value over the crack front. Furthermore, as can be seen in Fig. 3, at least the half of the crack front is submitted at values of *J*-integral close to the maximum registered at the center of the defect. This behavior of applied *J* over the crack front was also founded for the other cases considered. Therefore, the previous observation permits to use the maximum value of *J* (*J* at the center of the defect) as the characteristic crack loading parameter.

Once the crack front place from were the *J*-integral is considered as the crack loading parameter is defined, the effect of loading biaxiality on applied *J* can be studied. Figure 4 (a-b) presents *J*-integral evolution with curvature of the pipes characterized by the strains at the outer fiber and different levels of biaxiality caused by internal pressure. Figure 4 (a) corresponds to the pipe with defect of a=2 mm and c=6.66 mm and Fig. 4 (b) corresponds to the pipe with defect of a=7 mm and c=23.33 mm. The values of applied *J*-integral, in the both cases, are strongly affected by the biaxiality caused by internal pressure. For the same imposed curvature (characterized by strains at the outside fiber), internal pressure causes an important increment on applied *J*.

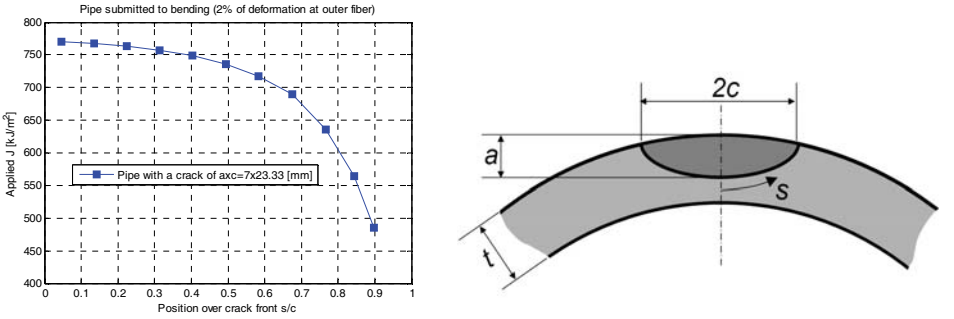

(a) (b)

Figure 3: a) Variation of applied *J*-integral along the crack front for the pipe with circumferential defect of a=7 mm and c=23.33 mm. b) Scheme of circumferential defect and definition of position along the crack front.

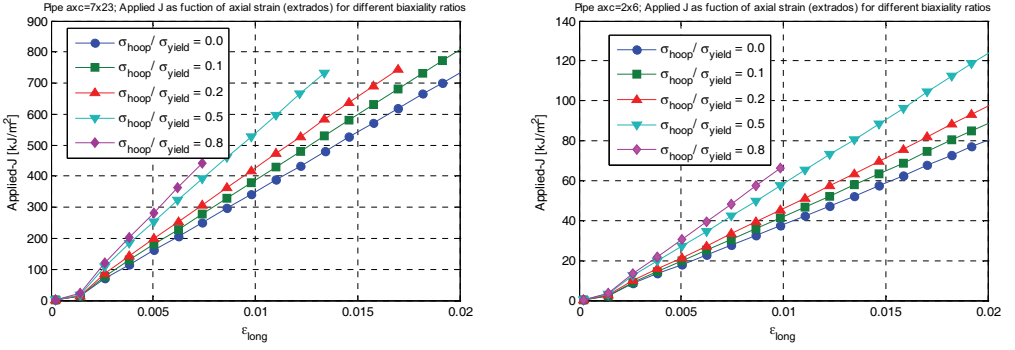

(a) (b)

Figure 4: a) Applied *J*-integral at the deepest point as a function of axial strain for different levels of biaxiality; pipe with defect of a =7 mm and c=23.33 mm; b) Applied *J*-integral at the deepest point as a function of axial strain for different levels of biaxiality; pipe with defect of a = 2 mm and c=6.66 mm.

Constraint Quantification

Constraint refers to the level of hydrostatic stresses ahead of the crack front under remote loading. In a specimen with finite dimensions, the boundary conditions strongly affect the crack-tip stress-strain fields. The stresses are generally lower than the stresses in an infinite cracked body. This phenomenon is often known as loss of crack tip constraint. When comparing differences in constraint between cracked configurations, questions arise about the precise definition of stress triaxiality and about the relevant position(s) ahead of the crack front at which such comparisons are made. The most common theory to characterize the loss of crack-tip constraint is the *J-Q* [1, 2] methodology.

The J-Q methodology

In this widely used methodology to compute the constraint loss, the stress field in a finite body is compared with the field from a reference solution constructed for small-scale yielding (*SSY*) conditions. Commonly the reference solution is the "*Boundary Layer"* (BL) model [4, 8]. O'Dowd and Shih (O&S) [1] proposed an approximate two-parameter description for the elastic-plastic crack-tip fields based upon a triaxiality parameter applicable under large scale yielding (*LSY*) conditions. Studying detailed numerical analyses employing the BL model O&S identified a family of self-similar fields in the form of

$$\sigma_{ij} = \sigma_0 \hat{f}_{ij}\left(\frac{r}{J/\sigma_0}, \theta, Q\right) \tag{3}$$

where the dimensionless Q parameter, defines the amount by which σ_{ij} in a finite body (*FB*) differs from the reference small scale yielding (*SSY*) solution.

Focusing the stress fields in the region ahead of the crack for the reference solution an the finite body (*FB*), O&S [1] showed that $Q\sigma_0$ corresponds to a spatial uniform hydrostatic stress, i.e., the d*ifference* field relative to a high triaxiality reference stress state

$$\sigma_{ij}^{FB} = (\sigma_{ij})_{SSY;T=0} + Q\,\delta_{1i}\delta_{1j}\;;\quad at:\ |\theta| < \frac{\pi}{2},\quad J/\sigma_0 < r < 5\,J/\sigma_0 \tag{4}$$

Operationally, Q is defined by

$$Q \equiv \frac{\sigma_{\theta\theta}^{FB} - \sigma_{\theta\theta}^{SSY}}{\sigma_0};\quad at:\ \theta = 0,\ \ r = \frac{2J}{\sigma_0} \tag{5}$$

where finite element analyses containing sufficient mesh refinement to resolve the fields at this length scale provide the finite body stresses. Here, it is noticed that Q is evaluated at $r = 2J/\sigma_0$ for definiteness. However, Q is virtually independent of distance in the range $J/\sigma < r < 5J/\sigma_0$.

The construction of a *J-Q* trajectory is done by the evaluation of Eq. (5) at each stage of loading in the finite body.

The *h* parameter for Constraint Characterization

The *J-Q* methodology is suitable to describe constraint condition in cleavage fracture because it only considers effects of constraint over the stress field developed ahead of the crack tip. However, it does not consider the effects of plastic deformations that are important in ductile fracture. The process of stable crack growth in metals can be divided in: 1) Nucleation of micro voids, 2) subsequent growth of the same voids, and 3) final coalescence of the micro voids [9]. Additionally, experimental observations and numerical simulations, demonstrated that plastic deformations associated to the process of void nucleation are small. This allows to simplify the failure process and to assume the growth of cavities as the critical event that controls the ductile tearing in metals.

Based on works of McClintock [10] and Rice and Tracey [11] that established the growth of micro voids as proportional to $\exp\left(3\sigma^{\infty}/2\sigma_0\right)$ where σ^{∞} and σ_0 are the remote hydrostatic stress and the yield stress respectively, Brocks and Schmitt [3] proposed the *h* parameter defined as the ratio of the hydrostatic stress over the effective (Von Mises) stress as a measure of crack tip constrain applicable to ductile fracture,

$$h = \frac{\sigma_h}{\sigma_e}. \tag{6}$$

Here, it is noticed that h is evaluated at $r = 2J/\sigma_0$ for definiteness and to be consistent with the evaluation of Q parameter.

Constraint evolution in 3D Geometries

Figure 5 (a) shows the J vs. $-Q$ trajectories generated under increased loading at locations over the crack front for the 3D model of the deep notch ($a/W = 0.5$) SENT specimen. Q is defined by Eq. (5) at the normalized distance ahead of the crack front given by $r = 2J/\sigma_0$. Q values from the SENT model reveal a loss of constrain upon loading. Also, Fig. 7 shows the constraint variation with the distance to the model centerplane. As the trajectories are closer to the free face of the specimen, the J-Q trajectories become more negative indicating a greater loss of constraint in this region which demonstrates the influence of the free face on the stress fields. However, the J-Q trajectories comprised in the 60% central portion of the crack front fall in a narrow band. This observation suggests that the J-Q trajectory corresponding to the center of the specimen is representative of the constraint conditions of this geometry.

Now, Fig. 5 (b) shows the J vs. h trajectories generated under increased loading at locations over the crack front for the 3D model of the deep notch ($a/W = 0.5$) SENT specimen. The parameter h is defined in Eq. (6) at the normalized distance ahead of the crack front given by $r = 2J/\sigma_0$. As in the Q parameter, h values from the SENT model reveal a loss of constrain upon loading. Furthermore, as the J-h curves approximate the model free face, the h values are closer to zero indicating a greater loss of constraint in this region which demonstrates the influence of the free face in the stress fields. However, for J-h trajectories comprised in the 60% central portion of the crack front, this variation over the crack front is not evident. This observation suggests that the J-h trajectory corresponding to the center of the specimen is representative of the constraint conditions in this geometry. The same observations were made for the shallow cracked SENT specimen and for the circumferentially cracked pipes. For these cases the graphs are not included here to save space.

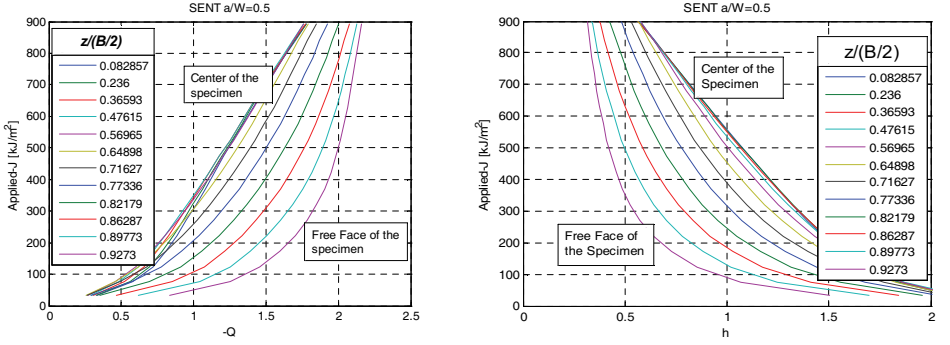

(a) (b)

Figure 5: J-Q trajectories for the 3D SENT model with $a/W = 0.5$ at different crack front locations; b) J-h trajectories for the 3D SENT model with $a/W = 0.5$ at different crack front locations.

Effect of Biaxiality on Constraint Levels of Pipes and Comparison with SENT

The parameters Q and h obtained from the middle point of the crack front are representative of the constraint conditions in the studied geometries. The J-Q and J-h curves of SENT specimens and cracked pipes under different biaxial conditions were compared. Figure 6 (a) shows the evolution of parameter Q with crack-tip loading, J, (both values obtained at the center of the crack front) for the clamped SENT specimen against the cracked pipe with $a/t = a/W = 0.5$. Figure 6 (b) shows the same results for relative crack size, $a/t = a/W = 0.15$. These analyses show good agreement between the SENT and the pipe level of constraint for the both crack sizes considered. Furthermore, from Fig. 6 (a-b), it can be established that the biaxial loading does not significantly modify the level of constraint for the range of loadings considered here.

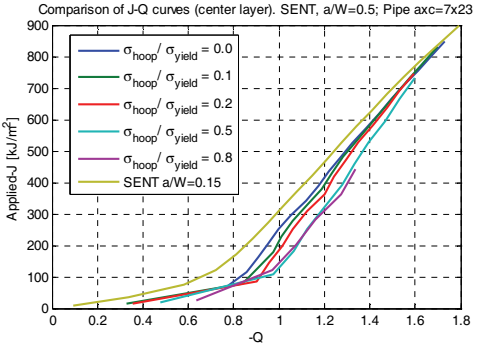

(a)

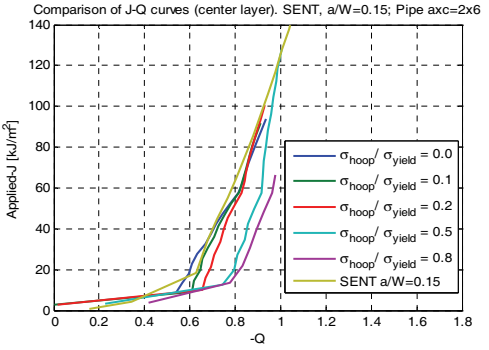

(b)

Figure 6: Comparison of J-Q curves between SENT specimen and cracked pipe with different biaxiality levels for: a) $a/W = a/t = 0.5$ and b) a) $a/W = a/t = 0.15$.

In the same way it was done with the J-Q trajectories, Fig. 7 (a-b) compares the evolution of parameter h with crack-tip loading, J, (both values obtained at the center of the crack front) for the clamped SENT specimen against the cracked pipe. The J-h trajectories consider equal relative crack sizes for the SENT specimens and cracked pipes ($a/W = a/t = 0.5$ and 0.15). Again, these analyses show a trend already observed in the previous Fig. 6 (a-b) with the Q parameter in which the clamped SENT specimen and the cracked pipes exhibit similar levels of crack-tip constraint for the both crack sizes considered. Furthermore, as in the previous analyses with the Q parameter, from Figs. 7 (a-b), it can be established that the biaxiality level does not significantly modify the level of constraint for the range of loadings considered here.

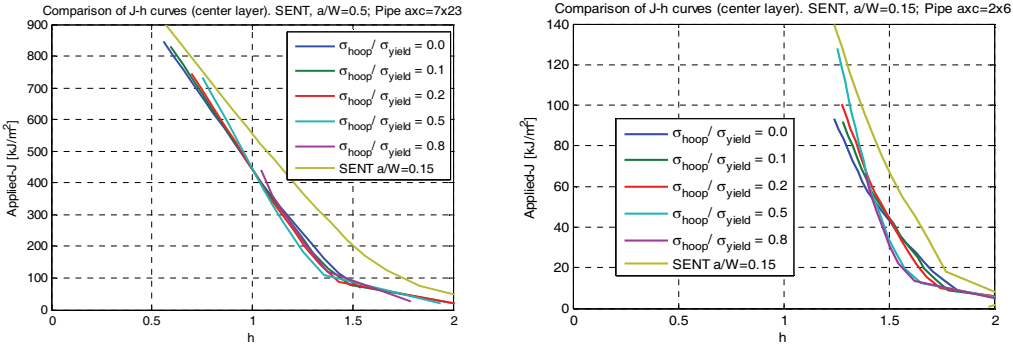

(a) (b)

Figure 7: Comparison of *J-h* curves between SENT specimen and cracked pipe with different biaxiality levels and $a/W = a/t = 0.5$; b) Comparison of *J-h* curves between SENT specimen and cracked pipe with different biaxiality levels for: a) $a/W = a/t = 0.5$ and b) a) $a/W = a/t = 0.15$.

Biaxiality Effects on J-R curves

To study the effect of biaxial loading on ductile tearing of materials, this section presents results from crack growth simulations. A model for a semielliptical surface cracked plate under different levels of biaxial loading, as described in previous section, is employed in the analysis. Figure 8 (a) presents crack growth as function of local applied *J*-integral at different positions over the crack front for the plate without biaxial loading. As can be noticed the "locally" obtained resistance curves are very similar for the different crack front positions. Similar behavior was found for the plate with different biaxial levels.

Figure 8 (b) compares the crack growth as a function of J-integral at the center of the semielliptical crack for different biaxial levels. The parameter to describe crack growth is the increment of crack depth (a) at the center of the semielliptical crack. Furthermore, the selected parameter to characterize the crack driving force was the applied J-integral at the center of the crack. As can be seen, the obtained resistance curve is not significantly affected by the biaxiality level. These results demonstrate the small influence of biaxial loading in the fracture resistance curve.

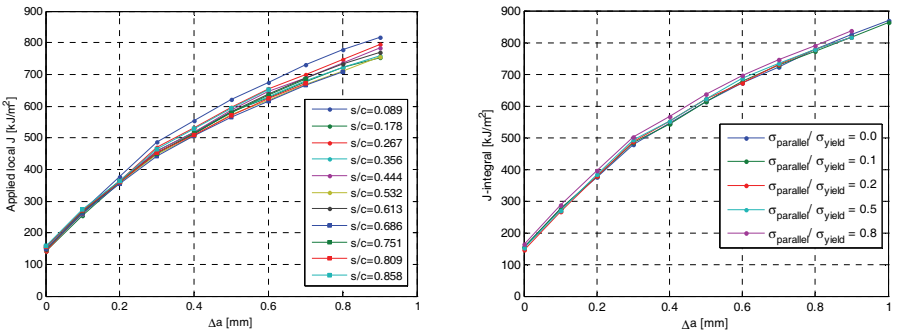

(a) (b)

Figure 8: a) Comparison of crack growth as a function of J-integral for different positions over the crack front; b) Comparison of crack growth as a function of J-integral at the center of the semielliptical crack for different biaxial conditions.

Discussion and Conclusions

By means of finite element modeling, the effect of biaxial loading on applied *J*-integral and level of constrain was studied. Pipes submitted to bending and internal pressure were considered. The applied *J*-integral is significantly influenced by the internal pressure. On the other hand, the levels of constraint ahead of the crack tip are not sensibly modified by the biaxial loading. This fact was verified by the use of the hydrostatic parameter Q and the ratio of the hydrostatic stress over the Von Mises stress h. Furthermore, 3D simulations for stable crack growth using the computational cell methodology, provides additional evidences to the small effect of biaxial loading condition on resistance curve for pipeline steels.

The small differences found in the constraint levels of SENT and pipes for the different biaxial levels and the stable crack growth simulations for a surface cracked plate, indicate that the resistance curve obtained from uniaxial loading can be also applied to biaxial loading situations. This provides additional support to previous results presented by E. Østby and A. O. Hellesvik [12] where full scale test of pipes submitted to bending and different degrees of internal pressure demonstrated the small effect of biaxiality on resistance curves.

Furthermore, for the same relative crack deep, constraint comparison of SENT specimens and pipes indicate the similarity in the fracture condition of these geometries. This result validates the use of SENT specimens in fracture characterization of circumferentially cracked pipes as well when the pipe is submitted to biaxial loading.

References

[1] O'Dowd NP, Shih CF., 1991, " Family of crack-tip fields characterized by a triaxiality parameter: Part I – structure of fields," *J Mech Phys Solids*, Vol.39, pp.989-1015.
[2] O'Dowd NP, Shih CF, 1992, "Family of crack-tip fields characterized by a triaxiality parameter: Part II – fracture applications," *J Mech Phys Solids*, Vol.40 pp. 939-63.
[3] W. Brocks and W. Schmitt, 1993, "Quantitative Assessment of the Role of Crack Tip Constraint on Ductile Tearing," *Constraint Effects in Fracture, ASTM STP 1171*, American Society for Testing and Materials, pp. 64-78.
[4] Rice, J. R., 1967, "Mechanics of Crack Tip Deformation and Extension by Fatigue**,"** *Fatigue Crack Propagation, ASTM STP 415,* American Society for Testing and Materials, pp. 247−309.
[5] Koppenhoefer K, Gullerud A, Ruggieri C, Dodds R, Healy B., 1994, "WARP3D: Dynamic nonlinear analysis of solids using a preconditioned conjugate gradient software architecture," *Structural research series (SRS) 596, UILU-ENG-94-2017*, University of Illinois at Urbana-Champaign.
[6] Xia, L. and Shih, C. F., 1995, ''Ductile Crack Growth − I. A Numerical Study Using Computational Cells with Microstructurally Based Length Scales", *Journal of the Mechanics and Physics of Solids*, Vol. 43, pp. 233−259.
[7] Ruggieri, C. and Dodds, R. H., 1996, "Numerical Modeling of Ductile Crack Growth in 3-D Using Computational Cell Elements," *International Journal of Fracture*, Vol. 82, pp. 67-95.
[8] Larsson, S. G. and Carlsson, A. J., 1973, "Influence of Nonsingular Stress Terms and Specimen Geometry on Small Scale Yielding at Crack Tip in Elastic−Plastic Materials," *Journal of Mechanics and Physics of Solids*, Vol. 21., pp. 263−277.
[9]. Garrison, W. M. Jr., Moody, N.R., 1987 "Ductile Fracture," *Journal of the Physics and Chemistry of Solids*, Vol. 48, pp. 1035−1074.
[10] McClintok, F. A., 1968, "A Criterion for Ductile fracture by the Growth of Holes," *Transaction of the ASME, Journal of Applied Mechanics*, Vol. 35, pp. 363-371.
[11] Rice J. R., Tracey D. M., 1969, "On the Ductile Enlargement of Voids in Triaxial stress Fields," *Journal of Mechanics and Physics of Solids*, Vol. 17, pp. 201-217.
[12] E. Østby and A. O. Hellesvik, 2007, "Fracture Control – Offshore Pipelines JIP Results from large scale testing of the effect of biaxial loading on the strain capacity of pipes with defects," *Proceedings of the Seventeenth International Offshore and Polar Engineering Conference ISOPE2007*, Lisbon, Portugal.